Aerodynamic Analysis of NACA64A010 Airfoil Using XFLR5 and ANSYS Fluent

Dinh Van Thin[1], Nguyen Huu Duc[1,*], and Le Quang Sang[2]

ARTICLE INFO

Article history:
Received: 10 November 2022
Revised: 14 March 2023
Accepted: 19 April 2023

Keywords:
NACA64A010 Airfoil
Low Reynolds Number
Angle of Attack
AoA
XFLR5
ANSYS Fluent

ABSTRACT

This paper presents the aerodynamic analysis results of the NACA64A010 airfoil model by two different methods: the Panel Method (PM) and the Computational Fluid Dynamics (CFD) method. The PM is performed on XFLR5 code, while the CFD is executed on ANSYS Fluent software. The NACA64A010 airfoil model will be analyzed under various conditions of Reynolds numbers and angles of attack (AoA). Reynolds numbers are 61700, 101700, 203100 and 308400, and AoA values will be changed between -6.5º and 8.0º, respectively. Then some main parameters such as lift coefficient C_l, drag coefficient C_d and the rate of (C_l/C_d) will be collected for all models. The simulated results obtained by both methods have slightly different deviations in comparison with the experimental values. According to these models, ANSYS Fluent brings the results closer to the experiment in all the considered ranges, however the XFLR5 only gives the appropriated results in cases of low Reynolds number. In contrast, the values received from XFLR5 are more incorrect when Reynolds number increases. Obviously, we can conclude that the ANSYS Fluent with suitable meshing and boundary conditions will be more reliable than XFLR5 in cases of airfoil simulation.

1. INTRODUCTION

In recent years, the Vietnamese Government has paid great attention and facilitated the development of renewable energy sources towards the goal of sustainable development. Especially, the wind power development programs are bringing thousands of MW of clean electricity to serve domestic demands and export to neighboring countries [1, 2].

However, the development of wind power projects in Vietnam is mainly commercial operation. Investors often buy products from foreign partners and bring them to domestic potential locations for installation and operation. Until now, there have been many incidents and accidents related to the construction and operation of wind turbines, causing huge economic losses. The reason for this situation is largely due to the fact that we have skipped the necessary stages of scientific research before building the projects.

Currently, researching on wind power technology in the world is mainly in the direction of changing the design of turbine blades to bring the highest performance depending on actual operating conditions. There are many groups that have published research results showing the change of airfoil design according to operating conditions. For example, the study of the effect of a single leading-edge protuberance on NACA63$_4$-021 airfoil performance made by Chang Cai et al. [3]. Ji Yao et al. analyzed the aerodynamic performance of NACA0018 airfoil under different turbulence models [4]. In addition, many studies on adjusting the mathematical model to analyze and predict better aerodynamic characteristics to improve performance [5] – [8].

With the aim of introducing and comparing the modern analytical methods widely used in wind power technology, especially related to turbine blade design, our research team conducted a study to analyze the aerodynamic characteristics of the NACA64A010 airfoil model. In this study, the team used the two most modern analytical methods available today to perform and then compare the results with previously published experiments [9]. From the results of this study, the team also made some important remarks and points of attention when analyzing at different Reynolds number and AoA values during the actual operation of the turbine blades. The Reynolds numbers are 61700, 101700, 230100 and 308400, and the AoA range will vary from -6.5º to 8.0º, respectively.

2. RESEARCH METHODS

In this study, we used two different methods to simulate and analyze the aerodynamic characteristics of the NACA64A010 airfoil model. The NACA64A010 model has

[1]*Electric Power University, Hanoi, 100000, Vietnam.*
[2]*Institute of Energy Science - Vietnam Academy of Science and Technology, Hanoi, 100000, Vietnam.*
**Corresponding author:* Nguyen Huu Duc; Phone: +84-901008555; Email: ducnh@epu.edu.vn

a chord line (C) connecting the beginning and ending points is C=0.3048m, the maximum thickness (T) is T=0.03048m at position 0.4C. It is a symmetrical model, hence the maximum camber (M) of the sample M=0% [10]. The specifications of the NACA64A010 pattern are collected and converted to a file format that matches the input file requirements of each software. The typical geometric parameters of an airfoil model as shown in the Figure 1.

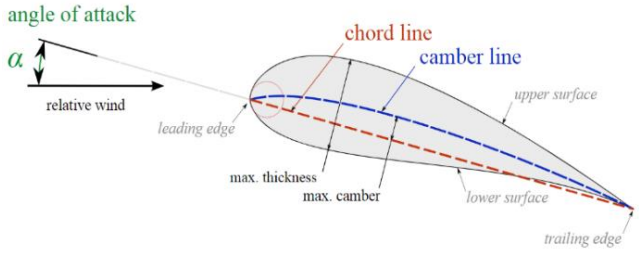

Fig. 1. Geometric parameters of airfoil [11].

2.1. XFLR5 code

XFLR5 code developed by Mark Drela and Harold Youngren is based on Xfoil, so the mathematical models of the two software are the same. The analysis capabilities for turbine blades was given by Matthieu Scherrer in version 2.0, initially using the Non-linear Lifting Line Theory (LLT), later using the Vortex Lattice Method (VLM) because the wing shapes have a more complex forms. Currently, the PM method was introduced in version 4.0 for both wing and plane analysis [12].

Considering the case where the flow is incompressible, inviscid and irrotational, the velocity potential equation can be shown in the form of Laplace's equation as following [13]:

$$\nabla^2\Phi^* = 0 \tag{1}$$

With Φ^* is the velocity potential equation at any point in the fluid field and can be expressed:

$$\Phi^*(x,y,z) = \frac{1}{4\pi}\int_{S_B+S_W}\mu\frac{\partial}{\partial n}\left(\frac{1}{r}\right)dS - \frac{1}{4\pi}\int_{S_B}\sigma\frac{1}{r}dS + \Phi_\infty \tag{2}$$

where, Φ is the perturbation potential; S_B, S_W are integral boundaries of blade and wake areas, m^2; μ, σ are the strength of doublets and sources; n is the normal vector.

The velocity of the stream at any position will be determined through Euler's formula:

$$\vec{V} = \nabla\Phi^* \tag{3}$$

In case of thin airfoils, to solve Laplace's equation (1) for the outside flow of the blades, the Dirichlet boundary condition must be used:

$$\Phi^*_{in} = \left(\Phi + \Phi_\infty\right)_{in} = const \tag{4}$$

When we set the inlet value for the velocity potential of internal flow, $\Phi^*_{in} = \Phi_\infty$, this condition means that the potential flow inside the blades is always constant. In the case of airfoil analysis, because there is no flow inside the airfoil, the turbulent flow inside the airfoil surface is zero. From formula (2) we have:

$$\frac{1}{4\pi}\int_{S_B+S_W}\mu\frac{\partial}{\partial n}\left(\frac{1}{r}\right)dS - \frac{1}{4\pi}\int_{S_B}\sigma\frac{1}{r}dS = 0 \tag{5}$$

The magnitude of the disturbance source component is determined through the Neumann boundary condition at each position on the surface of the airfoil:

$$\frac{\partial\Phi}{\partial n} = -\vec{n}.\overrightarrow{V_\infty} = -\sigma \tag{6}$$

Substituting equation (6) into equation (5), we will get the doublet strength component, from which, the velocity value at each point can be determined according to formula (3).

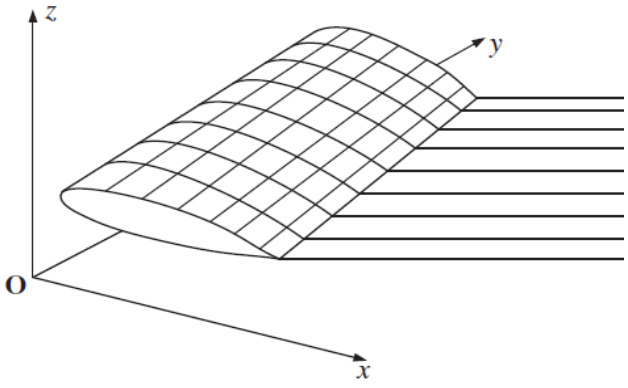

Fig. 2. Panel model for a blade [11].

The Figure 2 shows how the blade surface is divided according to the PM method, the blade surface is divided into N panels and the wake component is divided into N_W panels. The points satisfying the boundary condition will be assigned at the center of each panel. In this study, the airfoil sample NACA64A010 was divided into N=199 panels and N_W=0 panel.

According to the Bernoulli equation, the pressure factor at the kth panel is determined as follows:

$$C_{pk} = 1 - \frac{V_k^2}{V_\infty^2} \quad (7)$$

We have the aerodynamic load at the k[th] panel determined by the formula:

$$\Delta\overrightarrow{F_k} = -C_{pk}\left(\frac{1}{2}\rho V_\infty^2\right)\Delta S_k \overrightarrow{n_k} \quad (8)$$

where, V_k is the velocity at the center of the k[th] panel, m/s; ΔS_k is the area of the k[th] panel, m^2; ρ is the density of the air, kg/m^3.

We will get the lift coefficient C_l and drag coefficient C_d at the k[th] panel position when analyzing the force vector $\nabla\overrightarrow{F_k}$ along the coordinate axes corresponding to the wind direction to the blades.

2.2. ANSYS Fluent software

ANSYS Fluent is a state-of-the-art analysis program for fluid flow, heat transfer, and chemical reaction problems in complex geometric models. In the analysis of blade samples, we used the Reynolds-Averaged Navier – Stokes (RANS) method in ANSYS Fluent. In addition, we also need to add suitable turbulent models for the boundary conditions of each problem. The basic steps required for analysis on ANSYS Fluent are shown in Figure 3 [14].

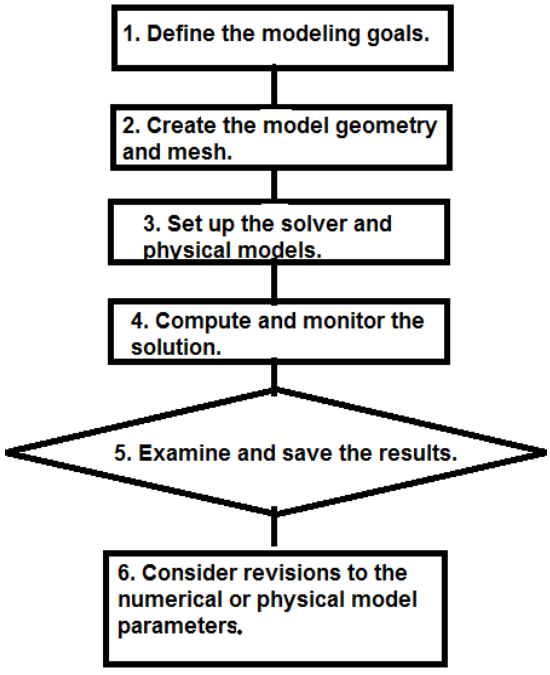

Fig. 3. The basic steps for analysis on ANSYS Fluent.

The system of Navier - Stockes equations, also known as control equations, consists of three fundamental conservation laws: conservation of mass, conservation of momentum and conservation of energy. In this study, the NACA64A010 airfoil was modeled in two dimensions and there was no additional energy exchange. The remaining conservation equations are expressed as in equations (9) and (10) as follows [15, 16]:

The continuity equation:

$$\frac{\partial V_j}{\partial x_j} = 0 \quad (9)$$

The momentum equation:

$$\rho\frac{\partial\left(V_j V_i\right)}{\partial x_j} = -\frac{\partial p}{\partial x_i} + \frac{\partial}{\partial x_j}\left[\left(\mu+\mu_T\right)\left(\frac{\partial V_i}{\partial x_j}+\frac{\partial V_J}{\partial x_i}\right)+\frac{2}{3}\rho k\delta_{ij}\right] \quad (10)$$

With: x_i, x_j are coordinate axes, respectively; V_i, V_j are the velocity vector along the coordinate axes, respectively, m/s; ρ is the density of the air, kg/m^3; p is the air pressure, Pa; μ is the dynamic viscosity of the air, Pa.s; μ_T is the turbulent eddy viscosity, Pa.s; k is the turbulent kinetic energy, J/kg.

In this study, the Spalart-Allmaras (S-A) turbulent model will be used, whereby the model will ignore the kinetic energy term of the turbulent flow, k, and only care about the turbulent eddy current viscosity term. According to Boussinesq's eddy viscosity hypothesis, the eddy current viscosity is determined as follows [17, 18]:

$$\mu_T = \mu^* f_{v1};\ f_{v1} = \frac{\chi^3}{\chi^3 + c_{v1}^3};\ \chi = \frac{\mu^*}{\mu} \quad (11)$$

where, μ^* is a working variable of the S-A model and obeys the transport equation:

$$\frac{D\mu^*}{Dt} = P - D + T + \frac{1}{\sigma}\left[\nabla.\left(\left(\mu+\mu^*\right)\nabla\mu^*\right)+c_{b2}\left(\nabla\mu^*\right)^2\right] \quad (12)$$

With the production term:

$$P = c_{b1}\left(1-f_{t2}\right)S^*\mu^* \quad (13)$$

The wall destruction term:

$$D = \left(c_{w1}f_w - \frac{c_{b1}}{\kappa^2}f_{t2}\right)\left(\frac{\mu^*}{d}\right)^2 \quad (14)$$

and the trip term is:

$$T = f_{t1}\left(\Delta u\right)^2 \quad (15)$$

We define S^* is the modified vorticity:

$$S^* = S + \frac{\mu^*}{\kappa^2 d^2} f_{v2} \; ; \; f_{v2} = 1 - \frac{\chi}{1 + \chi f_{v1}} \tag{16}$$

Where: S is the vorticity magnitude; d is the range to the closest wall; the f_w, f_{t1}, f_{t2} function are shown as follows:

$$f_w = g\left[\frac{1+c_{w3}^6}{g^6 + c_{w3}^6}\right]^{1/6}; g = r + c_{w2}\left(r^6 - r\right); r = \min\left(\frac{\mu^*}{S^* \kappa^2 d^2}, r_{\lim}\right) \tag{17}$$

$$f_{t1} = c_{t1} g_t \exp\left(-c_{t2} \frac{\omega_t}{\Delta u^2}\left[d^2 + g_t^2 d_t^2\right]\right) \tag{18}$$

$$f_{t2} = c_{t3} \exp\left(-c_{t4} \chi^2\right) \tag{19}$$

Here: $g_t = \min\left(0.1, \Delta v / \omega_t \Delta x\right)$; d_t is the distance to the trip point; ω_t is the vorticity at the trip point; Δv is the difference in velocity relative the trip point; Δx is space grid at the trip.

The constants used in the S-A model are:

$c_{b1} = 0.1355; \sigma = 2/3; c_{b2} = 0.622; \kappa = 0.41; c_{w1} = 3.239; c_{w2} = 0.3;$

$c_{w3} = 2; c_{v1} = 7.1; c_{t1} = 1; c_{t2} = 2; c_{t3} = 1.2; c_{t4} = 0.5; r_{\lim} = 10$

The boundary conditions are established for μ^*: in case of no-slip wall: $\mu^* = 0$ and in case of symmetry plane: $\partial \mu^* / \partial n = 0$.

3. RESULTS AND DISCUSSION

After collecting data on the shape of the NACA64A010 airfoil model [9], the authors converted it into a file suitable for the input file of each software and carried out the steps to build up and analyze the model. For XFLR5 software, the NACA64A010 pattern needs to be normalized to chord size C=1m, and then divided into 199 panels.

Fig. 4. The NACA64A010 model when inserted into XFLR5.

The relationship formula between Reynolds number and the chord size of the airfoil pattern is given as follows [9]:

$$\mathrm{Re} = \frac{\rho V_\infty C}{\mu} \tag{20}$$

From the formula (20), we have the corresponding conversion values of the Reynolds numerical values depend on chord size as shown in the Table 1.

For analysis on ANSYS Fluent, after successfully importing the geometry file of NACA64A010, we need to build more outside space around the airfoil to be able to set the conditions suitable for the model. The radius of the front space of the airfoil pattern is 6m and the surrounding space is rectangular in shape with sides of 12m and 18m respectively as shown in the Figure 5.

Table 1. Conversion values of Reynolds number in case of chord size C=1m

μ, (kg/m.s)	ρ, (kg/m^3)	V_∞, (m/s)	Re	Re_C
1.79.10^{-5}	1.225	2.96	61700	202427.8
1.79.10^{-5}	1.225	4.87	101700	333661.4
1.79.10^{-5}	1.225	9.73	203100	666338.6
1.79.10^{-5}	1.225	14.61	304800	1000000.0

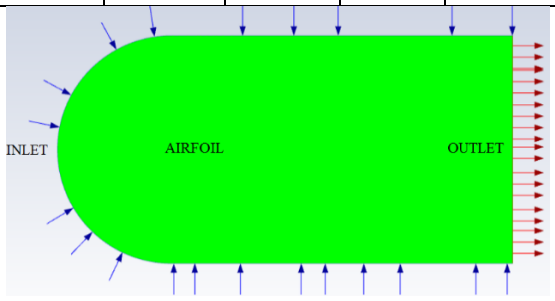

Fig. 5. The NACA64A010 model in ANSYS Fluent.

In the next step, the model is spatially meshed, the type of mesh used is a mixture of triangle and quadrilateral mesh with a minimum mesh size of 0.03m. The mesh layer surrounding the airfoil sample is divided into the quadrangular grids with 5 layers, the first layer has a thickness of 0.005m, each layer has a size difference of 1.1 times. Each different AoA will have a corresponding meshing model, the average number of meshes of each model is approximately 300000 elements and the mesh qualities in all cases are higher than 95%.

In order to select the above settings, we previously investigated the influence of the mesh size, the number of mesh elements, on the lift coefficient at a specific angle of attack, AoA= 5^o. The obtained results are shown in Table 2 and Figure 6. Initially, when the number of mesh elements is increased, the value of the lift coefficient also increases. However, when the mesh size is between 0.031m and 0.025m, the value of the lift coefficient is almost unchanged, the deviation between these values is less than 1%.

Therefore, we decided to use a grid size of 0.03m for all models in this paper.

Table 2. Lift coefficient depends on the number of grid cells at AoA=5º

No.	Element Size, m	Element Number	Lift Coefficient, c_l	Element Quality
1	0.090	34465	0.4424	0.927
2	0.080	43489	0.4481	0.931
3	0.070	56184	0.4608	0.936
4	0.060	75683	0.4717	0.940
5	0.045	133852	0.4739	0.945
6	0.040	168344	0.4731	0.953
7	0.031	278993	0.5048	0.956
8	0.030	298433	0.4967	0.957
9	0.028	341957	0.5078	0.956
10	0.025	433260	0.4976	0.966

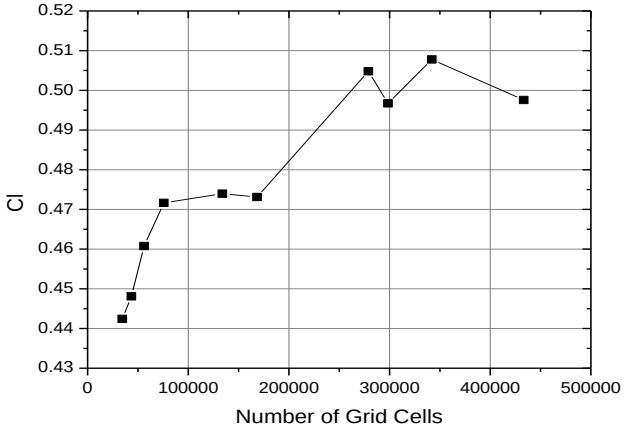

Fig 6. Lift coefficient depends on the number of grid cells at AoA=5º

In the solving setting progress, the front and two side walls of the outside space will be installed with the inlet boundary condition, while the back wall will be set as the outlet boundary condition of the model. In addition, the wall surrounding the airfoil will be set to the wall condition that is smooth and fixed as shown in the Figure 5. The solution method is pressure-velocity coupling using SIMPLE scheme. The turbulent model is Spalart-Allmaras (SA) one equation with strain or vorticity-based production. Finally, every particular model will be run with 1000 iterations to achieve appropriate convergence as illustrated in the Figure 7.

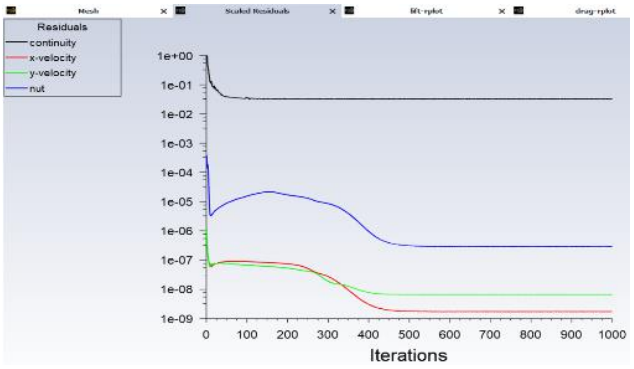

(a)

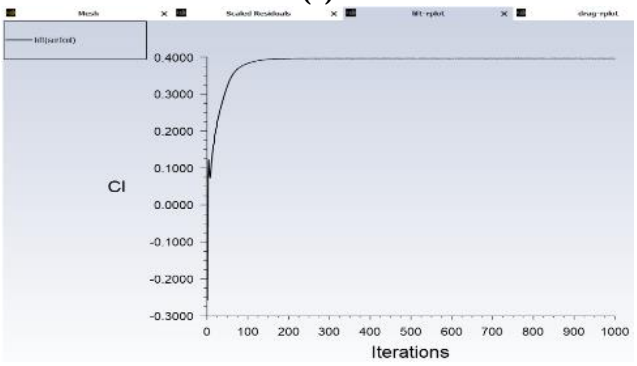

(b)

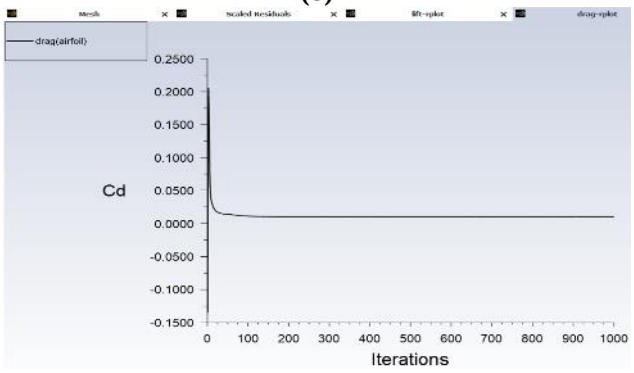

(c)

Fig. 7. (a) The scaled residuals, (b) lift coefficient and (c) drag coefficient during running progress.

In the field of wind turbine blade design, we are often interested in two quantities, the lift coefficient C_l and the drag coefficient C_d, which are determined by the following formula [9]:

The lift coefficient C_l:

$$C_l = \frac{l}{\frac{1}{2}\rho V_\infty^2 C} \tag{21}$$

And the drag coefficient C_d:

$$C_d = \frac{d}{\frac{1}{2}\rho V_\infty^2 C} \quad (22)$$

In the first case, the lowest Reynolds number is used, Re=61700 in ANSYS Fluent and Re=202427.8 in XFLR5, corresponding to an incoming air velocity value is: $V_\infty = 2.96$ m/s. The values obtained from the simulation of the two types of software are compared with the experimental measurement results shown in the Figure 8.

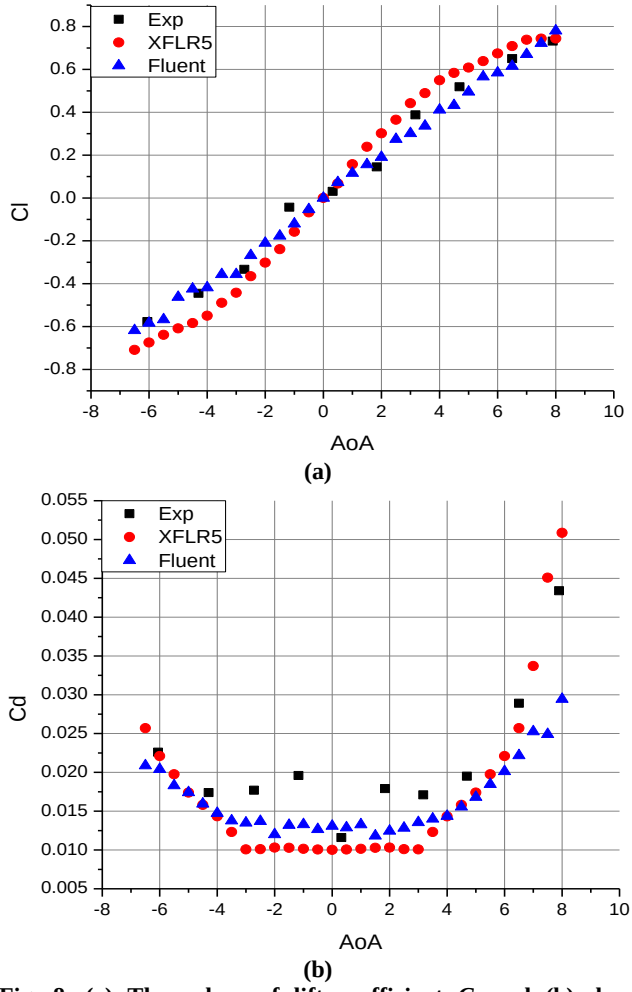

Fig. 8. (a) The values of lift coefficient C_l and (b) drag coefficient C_d vary with AoA.

From the Figure 8(a), we see that the lift coefficients C_l simulated from both XFLR5 and ANSYS Fluent are close to the experimental points. Similarly, the simulation results for the drag coefficients C_d from both codes are quite similar to the experimental measured value as shown in the Figure 8(b). However, the simulated Cd values at the AoA from -4° to +4° have a significant deviation in comparison with the experimental values.

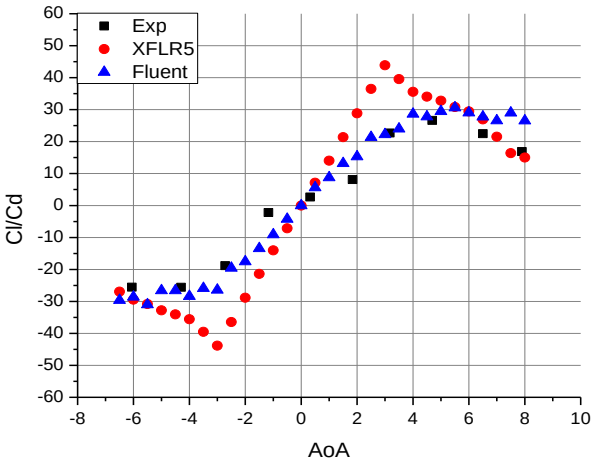

Fig. 9. The C_l/C_d ratios vary with AoA.

The ratio between the lift coefficient C_l and the drag coefficient C_d will be proportional to the operating power of the turbine blade, this value will tell us which AoA gives the best performance of the blade. From the Figure 9, we see that at neighboring angles AoA=0°, both codes give the good results. However, XFLR5 gives more skewed results at the angles AoA<-1° and AoA>+1°. Meanwhile, ANSYS Fluent still gives approximate values to the experiment at most values of AoA. According to the data in the Figure 9, the C_l/C_d ratio calculated from XFLR5 reached the highest value at the angle AoA=3°, but the measured values from experiment and ANSYS Fluent software both give maximum values at AoA=5°.

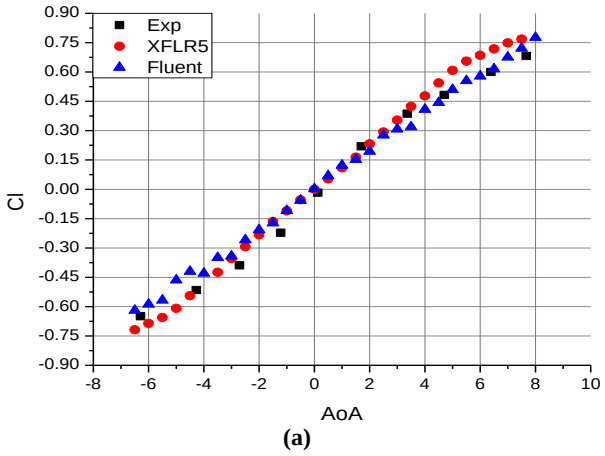

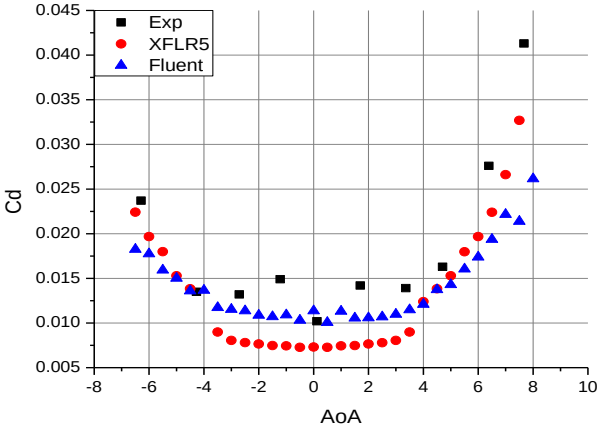

(b)

Fig. 10. (a) The values of lift coefficient C_l and (b) drag coefficient C_d vary with AoA.

When the Reynolds number increases, Re=101700 in ANSYS Fluent and Re=333661.4 in XFLR5, which equates to an inflow velocity of 4.78 m/s. Similar to the first case, the values of lift coefficient C_l between simulation and experiment are still very similar as shown in the Figure 10(a). However, when considering the value of drag coefficient C_d, ANSYS Fluent gives more accurate results, but XFLR5 starts to tend to deviate more, especially in the region from AoA=-4° to AoA =+4° as shown in the Figure 10(b).

However, for the values of the ratio of C_l to C_d, XFLR5 showed simulation results closer to the experimental values. The differences between the simulation results of the two codes in this case have been narrower as shown in the Figure 11.

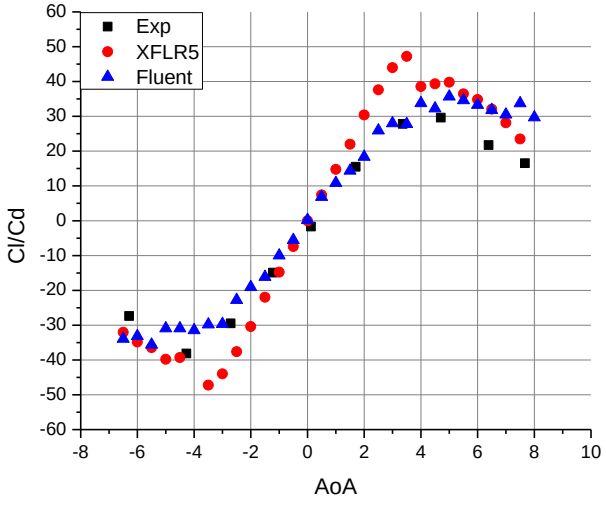

Fig. 11. The C_l/C_d ratios vary with AoA.

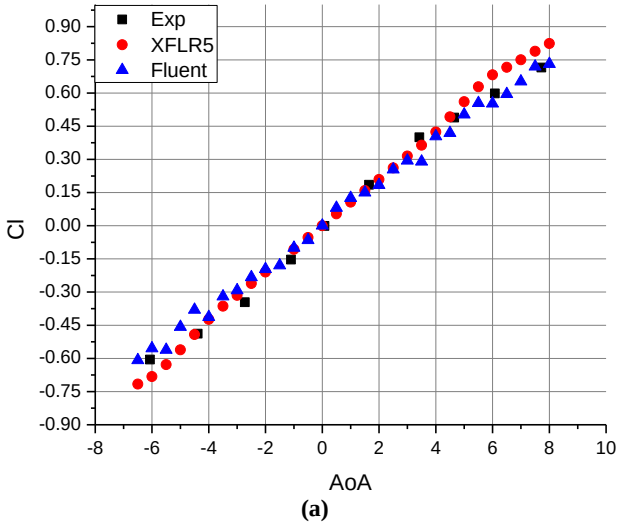

(a)

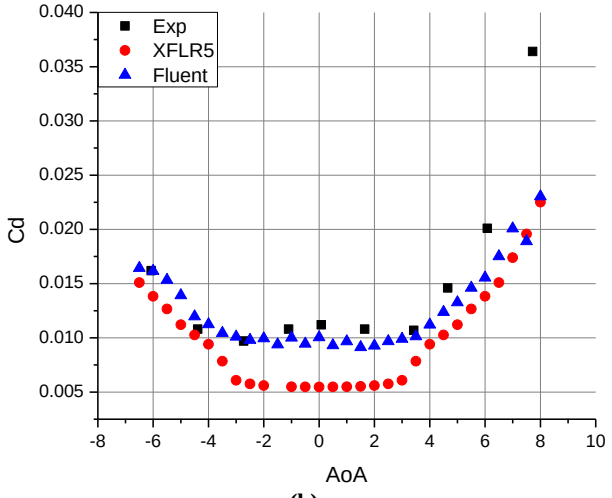

(b)

Fig. 12. (a) The values of lift coefficient C_l and (b) drag coefficient C_d vary with AoA.

When the incoming air flow velocity reaches 9.73 m/s, it corresponds to Re=203100 in ANSYS Fluent and Re=666338.6 in XFLR5. This speed value is classified as average and suitable for some areas of Vietnam.

From the Figure 12(b), we see that the C_d values obtained from XFLR5 are almost completely separate from the values obtained from the experiment. In contrast, ANSYS Fluent software gives increasingly accurate results and the deviation is almost negligible for both the lift coefficient C_l, the drag coefficient C_d and their ratio at all points of AoA as shown in the Figure 12 and the Figure 13. It is clear that, at higher velocity values, the larger Reynolds number, the differences between the two simulation codes become worth considering.

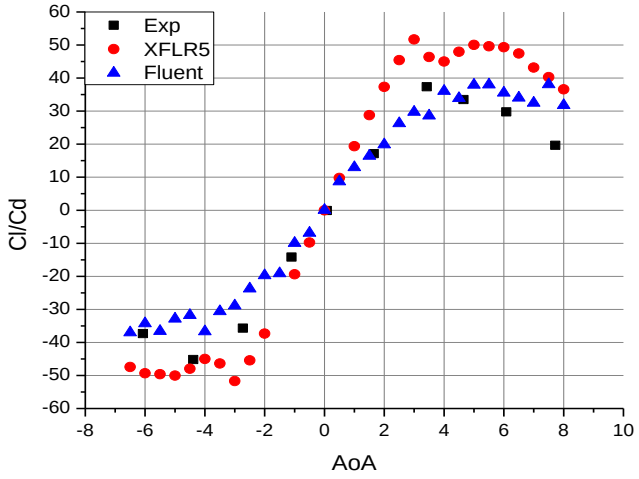

Fig. 13. The C_l/C_d ratios vary with AoA.

In the case of the largest Reynolds number, Re=304800 in ANSYS Fluent and Re=1000000 in XFLR5. The values of lift coefficient C_l obtained from both codes are still very accurate as shown in the Figure 14(a), however, in the Figure 14(b), the C_d values of XFLR5 are completely separate from those simulated by ANSYS Fluent and Experiments.

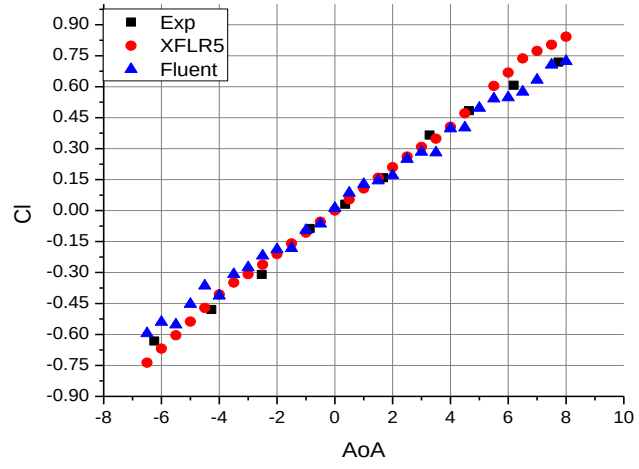

(a)

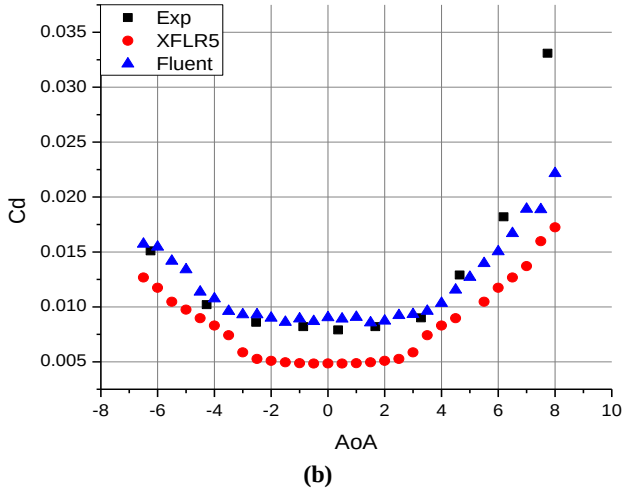

(b)

Fig. 14. (a) The values of lift coefficient C_l and (b) drag coefficient C_d vary with AoA.

For the ratios between the lift coefficient C_l and the drag coefficient C_d, the XFLR5 results are getting farther and farther away from the experiment as the Reynolds number increases as shown in the Figure 15.

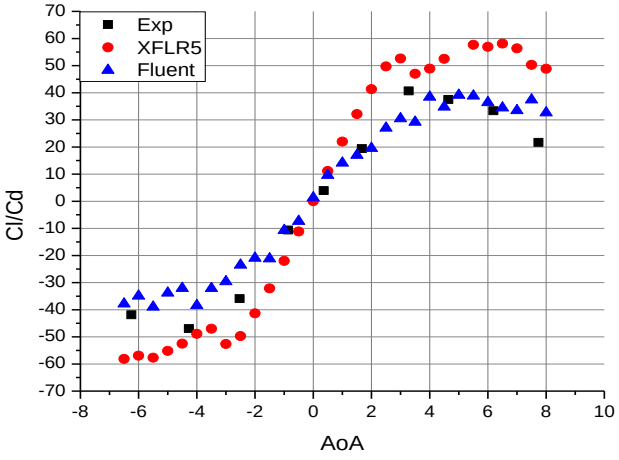

Fig. 15. The C_l/C_d ratios vary with AoA.

4. CONCLUSIONS

From the analysis in this paper, the authors can draw some conclusions as follows:

XFLR5 software should only be applied for preliminary analysis of the airfoil pattern at angles of attack in vicinity of 0^o due to the limitations of both the computational model and the PM meshing method. Besides, XFLR5 software should only analyze airfoil samples in cases where Reynolds number is less than Re=666338.6.

ANSYS Fluent software using the SA one equation turbulent flow model gives the results that are very

consistent with the experimental values at all angles of attack, however, at large angles of attack, the difference is also significant.

ACKNOWLEDGEMENT

This work was supported by Electric Power University and the Institute of Energy Science (IES) of the Vietnam Academy of Science and Technology (VAST).

This research is a result of the project funded by the Institute of Energy Science (IES) of the Vietnam Academy of Science and Technology (VAST) with Code VAST07.01/22-23.

REFERENCES

[1] Minh, Q. D.; Thanh, V. D.; Van, T. N.; Hong, V. P. N.; Ngoc, T. N. T.; and Thi, T. M. L. 2018. Effects of FSIG and DFIG Wind Power Plants on Ninh Thuan Power Grid, Vietnam. GMSARN International Journal 12 (3): 133 - 138.

[2] Nguyen, T. A.; and Nguyen H. D. 2022. Effect Analysis of Performance and Pitch Controller Operation for Wind Turbine under Rain. GMSARN International Journal 16 (4): 339-347.

[3] Chang, C.; Shuhong, L.; Zhigang, Z.; Takao, M.; Yasunari, K.; Qing'an, L.; and Ryota, S. 2019. Experimental and theoretical investigations on the effect of a single leading-edge protuberance on airfoil performance. Phys. Fluids 31 (2): 1 - 16. DOI: 10.1063/1.5082840.

[4] Ji, Y.; Weibin, Y.; Jianliang, W.; Jianbin, X.; Haipeng, Z.; Mingjun, P.; Yong, S. 2012. Numerical simulation of aerodynamic performance for two dimensional wind turbine airfoils. Procedia Engineering 31: 80 – 86.

[5] Xingxing, L.; Lei, Z.; Juanjuan, S.; Fengjiao, B.; Ke, Y. 2020. Airfoil design for large horizontal axis wind turbines in low wind speed regions. Renewable Energy 145: 2345-2357.

[6] Xiaoping, P.; Haoyu, W.; and Jin, C. 2019. Intelligence algorithm for optimization design of the low wind speed airfoil for wind turbine. Cluster Computing 22: 8119 - 8129. DOI:org/10.1007/s10586-017-1635-4.

[7] Stephen, K. M.; Kathrin, S.; Kevin, V.; Nicholas, K.; and Thomas, H. C. 2021. A design and performance prediction method for small horizontal axis wind turbines and its application. AIMS Energy 9 (5): 1043–1066. DOI: 10.3934/energy.2021048.

[8] Shwe, Y. W.; and Mongkol, T. 2021. Parametric Optimization of NACA 4412 Airfoil in Ground Effect Using Full Factorial Design of Experiment. ENGINEERING JOURNAL 25 (12): 9 - 19. DOI:10.4186/ej.2021.25.12.9.

[9] Michael, S. S.; James, J. G.; Andy, P. B.; and Philippe, G. 1995. Summary of Low-Speed Airfoil Data: Volume 1. Virginia: SoarTech Publications.

[10] Airfoil Tools. 2022. Naca64a010-il [On-line serial], Retrieved November 8, 2022 from http://airfoiltools.com/airfoil/details?airfoil=naca64a010-il.

[11] Wikipedia. 2022. Airfoil [On-line serial], Retrieved November 8, 2022 from https://en.wikipedia.org/wiki/Airfoil.

[12] TechWinder. 2019. Xflr5 tutorial Retrieved November 8, 2022 from http://www.xflr5.tech/xflr5.htm? fbclid=IwAR0XI-jGI2AjxOqbNSB5Vfr0OlP6Xd TWqLGD DtCls BFfv-CGxq92Iyy8KYo.

[13] Lan, Y.; Changchuan, X.; and Chao, Y. 2019. Geometrically exact vortex lattice and panel methods in static aeroelasticity of very flexible wing. Proceedings of the Institution of Mechanical Engineers Part G Journal of Aerospace Engineering 234 (3). SAGE Publishers. DOI: 10.1177/0954410019885238.

[14] ANSYS Inc. 2021. ANSYS Fluent User's Guide. USA: ANSYS Inc.

[15] Moses, O. P.; and Vincent, A. O. 2017. Computational Study of Aerodynamic Flow over NACA 4412 Airfoil. British Journal of Applied Science & Technology 21 (3): 1 - 11. DOI: 10.9734/BJAST/2017/31893.

[16] Kun, C.; Wei-wei, Y.; Jian-hu, W.; Rui-biao, G.; Yi-xiao, L. 2021. Bionic coupling design and aerodynamic analysis of horizontal axis wind turbine blades. Energy Sci. Eng. 9: 1826–1838. DOI: 10.1002/ese3.953.

[17] Steven, R. A.; Forrester, T. J.; and Philippe, R. S. 2012. Modifications and Clarifications for the Implementation of the Spalart-Allmaras Turbulence Model. Proceedings of the Seventh International Conference on Computational Fluid Dynamics (ICCFD7), 9-13 July. Big Island, Hawaii.

[18] Charles, W. J.; William, C. T.; and Christopher, J. R. 2019. Turbulence Model Implementation and Verification in the SENSEI CFD Code. Proceedings of the AIAA Scitech Forum, 7 - 11 January. San Diego, California: AIAAA Publishers. DOI: 10.2514/6.2019-2331.